Meteoritics & Planetary Science 39, Nr 8, 1343–1357 (2004)
Abstract available online at http://meteoritics.org

High-calcium pyroxene as an indicator of igneous differentiation in asteroids and meteorites

Jessica M. SUNSHINE,[1*] Schelte J. BUS,[2] Timothy J. McCOY,[3] Thomas H. BURBINE,[4] Catherine M. CORRIGAN,[3] and Richard P. BINZEL[5]

[1]Advanced Technology Applications Division, Science Applications International Corporation, Chantilly, Virginia 20151, USA
[2]University of Hawaii, Institute for Astronomy, Hilo, Hawaii 96720, USA
[3]Department of Mineral Sciences, National Museum of Natural History, Smithsonian Institution, Washington, DC 20560–0119, USA
[4]Laboratory for Extraterrestrial Physics, NASA Goddard Space Flight Center, Greenbelt, Maryland 20771, USA
[5]Department of Earth, Atmospheric, and Planetary Sciences, Massachusetts Institute of Technology, Cambridge, Massachussets 02139, USA
[*]Corresponding author. E-mail: sunshinej@saic.com

(Received 9 March 2004; revision accepted 21 April 2004)

Abstract–Our analyses of high quality spectra of several S-type asteroids (17 Thetis, 847 Agnia, 808 Merxia, and members of the Agnia and Merxia families) reveal that they include both low- and high-calcium pyroxene with minor amounts of olivine (<20%). In addition, we find that these asteroids have ratios of high-calcium pyroxene to total pyroxene of >~0.4. High-calcium pyroxene is a spectrally detectable and petrologically important indicator of igneous history and may prove critical in future studies aimed at understanding the history of asteroidal bodies. The silicate mineralogy inferred for Thetis and the Merxia and Agnia family members requires that these asteroids experienced igneous differentiation, producing broadly basaltic surface lithologies. Together with 4 Vesta (and its smaller "Vestoid" family members) and the main-belt asteroid 1489 Magnya, these new asteroids provide strong evidence for igneous differentiation of at least five asteroid parent bodies. Based on this analysis of a small subset of the near-infrared asteroid spectra taken to date with SpeX at the NASA IRTF, we expect that the number of known differentiated asteroids will increase, consistent with the large number of parent bodies inferred from studies of iron meteorites.

INTRODUCTION

Asteroids record the conditions and processes that were active in the early solar system. The study of asteroids and their meteoritic samples offers insights into conditions in the solar nebula, accretionary processes, and subsequent thermal and aqueous alteration of asteroids. Geochemical analyses of meteorites provide constraints on the timing and nature of their petrogenesis, while studies of asteroids add spatial and geologic context. Remote spectroscopic studies, both telescopic surveys and missions that explore specific bodies, provide a powerful tool for mapping the composition of the asteroid population, particularly when compared to laboratory-based spectra of well-characterized meteorites. To link meteorite petrogenesis to asteroidal context, we must seek petrologically significant discriminators among meteorites that can be detected remotely on asteroid surfaces.

High-calcium pyroxene is one of the most effective tracers of melting of a chondritic precursor. During early Fe, Ni-FeS and silicate partial melting, troilite, high-calcium pyroxene, and plagioclase are all preferentially incorporated in early partial melts from a chondritic precursor and, therefore, depleted in their residues. A search for any one of these minerals provides a useful probe of differentiation. In practice, troilite (Britt et al. 1992; Cloutis and Burbine 1999) and plagioclase (Adams 1968, and references therein) have weak or ambiguous spectral signatures at visible and near-infrared wavelengths. In contrast, high-calcium pyroxene has prominent near-infrared spectral absorption features (Adams 1974; Burns 1993). Meteorite analyses show that chondritic high-calcium pyroxene abundances are intermediate between those of the primitive achondrites (which are residues of partial melting) and eucrites (which crystallized from partial melts). Thus, high-calcium pyroxene in asteroids can act as a tracer of their igneous history.

Recent advances in instrumentation allow us to measure subtleties in near-infrared spectral features that were previously not resolvable. While the introduction of charge-coupled devices (CCDs) revolutionized asteroid studies at visible wavelengths in the 1980s, new-generation infrared

array detectors are now having an even greater impact on asteroid science. In particular, near-infrared spectrographs are being designed and built that can record asteroid spectra over the wavelength interval from 1 to 5 μm with the resolution and signal-to-noise needed for meaningful mineralogical studies. At the NASA Infrared Telescope Facility (IRTF), near the summit of Mauna Kea in Hawaii, a new state-of-the-art near-infrared imager and spectrograph called SpeX (Rayner et al. 2003) has already produced high signal-to-noise spectra covering the interval from 0.8 to 2.5 μm for hundreds of main-belt and near-Earth asteroids. When combined with visible-wavelength CCD spectra like those obtained during the Small Main-belt Asteroid Spectroscopic Survey (Xu et al. 1995; Bus and Binzel 2002), the SpeX data reveal spectral absorption features in asteroids at a level of detail never before possible. With high signal-to-noise and high spectral resolution data extending through the near-infrared, we are now able to directly resolve the presence of both high-calcium pyroxene (HCP) and low-calcium pyroxene (LCP) and, thus, use HCP/(HCP + LCP) ratios to remotely trace igneous processing on asteroids.

BACKGROUND

High-Calcium Pyroxene During Igneous Differentiation

The first melt produced from an ordinary chondrite occurs at ~950 °C at the Fe, Ni-FeS cotectic and is composed of 85 wt% FeS (troilite) (Kullerud 1963). When the temperature reaches ~1050 °C, melting of the silicate portion begins. The importance of high-calcium pyroxene can be understood by considering melting in the silica-undersaturated portion of the fosterite-silica-anorthite-diopside quaternary (forsterite/Fo-enstatite/En-anorthite/An-diopside/Di). In this system, melting begins at a eutectic in the plagioclase-En-Di system. This eutectic melt is highly enriched in both plagioclase (PLG) and high-calcium pyroxene (approx. ~2:1:1 PLG:HCP:LCP) (Morse 1980, and references therein). Subsequent melts become increasingly enriched in low-calcium pyroxene at the expense of both high-calcium pyroxene and plagioclase, since the bulk composition lies toward the forsterite corner in the quaternary. It is worth noting that a pigeonite field is also present in the system, and formation of exsolved high- and low-calcium pyroxene lamellae occurs upon slow cooling of pigeonite. Thus, troilite, high-calcium pyroxene, and plagioclase are all preferentially incorporated in early partial melts from a chondritic precursor and depleted from residues of partial melting. Not surprisingly, the Fe, Ni-FeS cotectic and plagioclase-pyroxene eutectic melts are immiscible and separate during igneous differentiation.

To investigate the effect of melting on the HCP/(HCP + LCP) ratio, we used the MELTS program (Ghiorso and Sack 1995; Asimow and Ghiorso 1998) to calculate the composition of the partial melt and residual solid for melting of the silicate portion of average H chondrite falls (Jarosewich 1990). Calculations were performed with fO_2 at iron-wüstite and a pressure of 1 bar, appropriate to melting in a small, metal-bearing asteroid. Our starting composition had an HCP/(HCP + LCP) ratio of 0.139 (Fig. 1). HCP/(HCP + LCP) ratios for the residual were calculated directly from MELTS, while the ratio for the partial melt was determined from a CIPW norm of the liquid. HCP/(HCP + LCP) ratios of the earliest partial melts approach 0.9, increase slightly until ~4% partial melting, and then decrease. HCP/(HCP + LCP) ratios >0.3 correspond to partial melting <30%. The residues become depleted in HCP and have low degrees of partial melting, with no HCP remaining in the residue by ~7% partial melting. These calculations suggest that the HCP/(HCP + LCP) ratio is a sensitive indicator of the degree of partial melting of a chondritic precursor and could be an important tool for deciphering the igneous history of differentiated asteroids.

While the theoretical basis for expecting asteroid and meteorite differentiation to produce dramatic changes in high-calcium pyroxene abundance is clear, the strongest evidence lies in analyses of meteorites that have experienced varying degrees of differentiation. High-calcium pyroxene is difficult to distinguish optically and is often intimately intergrown with other silicate phases, so reliable estimates of its abundance are relatively few. McSween et al. (1991) calculated normative mineralogies for ordinary chondrite bulk compositions, determining that diopside accounts for between 4.1 and 5.3 wt% in H, L, and LL ordinary chondrites or 13–20% of the total pyroxene component (diopside + hypersthene). This

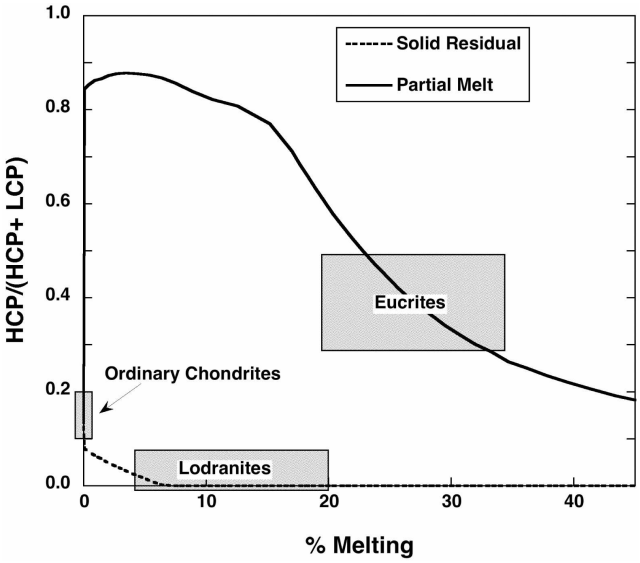

Fig. 1. HCP/(HCP + LCP) ratios in the solid residual and crystallized partial melt from an H chondrite precursor as a function of percent melting. Based on calculations of melting using the MELTS program (Ghiorso and Sack 1995; Asimow and Ghiorso 1998). HCP/(HCP + LCP) ratios greater than 0.3 are indicative of partial melts (e.g., eucrites), while ratios below 0.1 indicate residues (e.g., lodranites).

high-calcium pyroxene abundance may be broadly representative of a wide range of primitive chondrites. The Acapulco meteorite is thought to have experienced minimal silicate partial melting (McCoy et al. 1996), and it contains 4.4 wt% high-calcium pyroxene (~12% of the total pyroxene) (Palme et al. 1981). Thus, the range of HCP/(HCP + LCP) of ~10–20% appears typical for chondrites.

In contrast to chondrites, lodranites (which have experienced partial melting up to 20 vol% as well as melt migration) exhibit generally low HCP/(HCP + LCP) ratios. Modal analyses of lodranites consistently point to olivine as the dominant mineral, with high-calcium pyroxene depleted relative to chondrites. For example, the plagioclase-depleted lodranite Yamato-791491 contains 41.9% olivine, 28.0% low-calcium pyroxene, and 0.07% high-calcium pyroxene (Hiroi and Takeda 1991).

Conversely, eucrites are enriched in high-calcium pyroxene, consistent with their origin by crystallization of partial melts. Average basaltic eucrites (Delaney et al. 1984b) contain 12.3% augite, 19.2% pigeonite, and 19.7% orthopyroxene. If we group pigeonite with low-calcium pyroxene, consistent with their similar spectral behavior (Burns 1993), we find a HCP/(HCP + LCP) ratio of 24%; individual eucrites (e.g., Stannern; Delaney et al. 1984b) can range up to ratios of 42%. As a whole, the parent body of the howardite-eucrite-diogenite (HED) meteorites would exhibit lower values, consistent with the inclusion of orthopyroxene-rich, augite-poor diogenitic material with HCP/(HCP + LCP) ratios approaching zero.

The range in ratios between chondrites, residues of partial melting (lodranites), and crystallization products from the partial melts (eucrites) strongly suggests that the HCP/(HCP + LCP) ratio, when coupled with a measure of the olivine abundance, can be a powerful indicator of the igneous history of a meteorite or asteroid.

Deriving HCP/(HCP + LCP) from Spectra

Calcium-rich pyroxene is easily detected in reflectance spectra, given sufficient signal-to-noise and spectral resolution. Spectrally, low-calcium pyroxenes (which include pyroxenes of $Wo_{<5}$, with both ortho- and clino-structures, and pigeonites of $Wo_{5–15}$) are characterized by absorption features near both 1 and 2 μm. The absorptions arise from electronic transitions of Fe^{2+} ions in the M2 crystallographic site within the pyroxene structure (Burns 1993). High-calcium pyroxenes (augites and subcalcic augites with clino-structure and $Wo_{\sim>30}$), like low-calcium pyroxene, typically also have 1 and 2 μm absorption features from crystal field absorption due to Fe^{2+} in the M2 site. However, these absorptions in high-calcium pyroxene occur at longer wavelengths as larger Ca^{2+} ions replace Mg^2 in the M2 sites (Adams 1974; Cloutis and Gaffey 1991; Burns 1993). Calcium also preferentially fills the M2 site, and Fe^{2+} is, therefore, enriched in the M1 sites in high-calcium pyroxene. This gives rise to additional absorptions in HCP, the strongest of which is near 1.2 μm (Burns 1993; Schade et al. 2004).

Plagioclase and olivine also have major Fe^{2+} absorptions in the 0.4–2.5 μm region. Olivine has a complex absorption feature in the 1 μm region. This feature includes three absorptions that arise from crystal field transitions of Fe^{2+} in the M1 and M2 sites within the olivine structure (Burns 1993, and references therein). Each of these absorptions moves toward longer wavelengths with increasing Fe^{2+} content (Burns 1993; Sunshine et al. 2000), which causes the overall absorption feature to shift (King and Ridley 1987; Burns 1993). Changes in Fe/Mg also affect the relative strength of the M1 versus M2 absorption, which significantly alter the overall shape of the feature (Burns 1993; Sunshine et al. 2000). Finally, the 1 μm absorption feature in olivine is strongly affected by temperature (Singer and Roush 1985; Moroz et al. 2000; Sunshine et al. 2000; Hinrichs and Lucey 2002).

Although weaker than absorptions in olivine or pyroxene, Fe^{2+} in plagioclase also gives rise to an absorption near 1.2 μm (Burns 1993). This absorption has been identified in lithologies with large proportions of plagioclase, e.g., anorthosite outcrops on the Moon (Hawke et al. 2003) and on Vesta (McCord et al. 1970). However, this plagioclase absorption can easily be confused with the M1 absorption in high-calcium pyroxene, complicating mineralogical inferences.

The number and compositional variability of absorptions from major silicate minerals in the 1 μm and 2 μm regions present a significant interpretive challenge. In the 1 μm region, for example, there is significant overlap among absorptions from low-calcium pyroxene, high-calcium pyroxene, olivine, and plagioclase. Absorption band modeling was introduced in an attempt to mitigate many of these issues. In particular, Sunshine et al. (1990) developed an absorption band model based on a physical model of crystal field absorptions. This Modified Gaussian Model (MGM) has been shown to accurately model the shape of isolated absorptions and, thus, provides a high degree of confidence in resolving overlapping absorption bands (e.g., Mustard 1992; Sunshine and Pieters 1993, 1998; Schade and Wäsch 1999; Hiroi and Sasaki 2001; Ueda et al. 2003; Schade et al. 2004). Under the MGM, spectra are modeled in apparent absorbance (log reflectance using Beer's law) and energy as a series of modified Gaussian distributions superimposed onto a baseline continuum. Each absorption band is described by three model parameters: band center, width, and strength. The continuum is a straight-line in energy and is described by two additional parameters, a slope and an offset. Unlike traditional continuum removal techniques (e.g., Cloutis et al. 1986), the MGM continuum is not forced to be tangent to the spectrum but, rather, is optimized along with the absorption bands in the fitting process.

Of particular interest is the study by Sunshine and Pieters (1993), which used the MGM to model the spectra of a suite

of powders of known proportions of high- and low-calcium pyroxene. Consistent with crystal field theory (Burns 1993), spectra of mixtures of high- and low-calcium pyroxenes include five major absorptions: low- and high-calcium pyroxene each contribute a pair of M2 absorptions near 1 and 2 μm, with the fifth absorption due to the additional M1 band near 1.2 μm in high-calcium pyroxene. Sunshine and Pieters (1993) showed that as modal abundance varies, there is a systematic relationship between the HCP/(HCP + LCP) ratio and the relative strengths of HCP and LCP absorptions (Fig. 2) that is independent of particle size and is consistent whether measured in the 1 or the 2 μm regions. This relationship has been validated on a number of well-characterized laboratory samples, including an exsolved pyroxene crystal from Moses Rock Diatreme, Utah, containing exsolution lamellae of LCP and HCP (Sunshine and Pieters 1993), and the SNC meteorites (Sunshine et al. 1993; Schade and Wäsch 1999). The latter is particularly noteworthy. Pyroxenes in SNC meteorites are markedly enriched in FeO relative to those used to derive the end member spectra fit by MGM. Thus, the technique seems applicable to a broad range of pyroxene compositions. The ability of MGM to distinguish high- and low-calcium pyroxenes despite differences in the Fe/Mg ratio is not surprising, given the fact that changes in calcium produce larger spectral shifts than does iron (Adams 1974; Cloutis and Gaffey 1991; Burns 1993). It should be noted that pyroxenes that contain even small amounts of Ca include exsolved domains of high-calcium at some scale (e.g., in TEM; Camera et al. 2000, and in electron microscopy; Lorimer and Champness 1973). While in principal this might produce weak high-calcium bands in low-calcium pyroxene spectra, based on the studies described above, it apparently does not affect our ability to determine HCP/(HCP + LCP) ratios from spectra of mixtures of low- and high-calcium pyroxenes.

In applying MGM to understanding igneous differentiation, it is important to understand how expected high-calcium pyroxene abundances in various differentiated lithologies (Fig. 1) compare to our ability to detect differences in relative strengths of LCP/HCP bands (Fig. 2). Given the steepness of this relative band strength curve, detecting surfaces that have undergone high degrees of partial melting (>30%, e.g., eucrites) is relatively straightforward. (Although the steepness also implies uncertainties in inferring the precise HCP/[HCP + LCP] abundances for surfaces in this range.) At the other extreme, residual melts have <10% HCP/(HCP + LCP) and should be discernable from ordinary chondrites given the logarithmic scale of relative strengths of pyroxene bands.

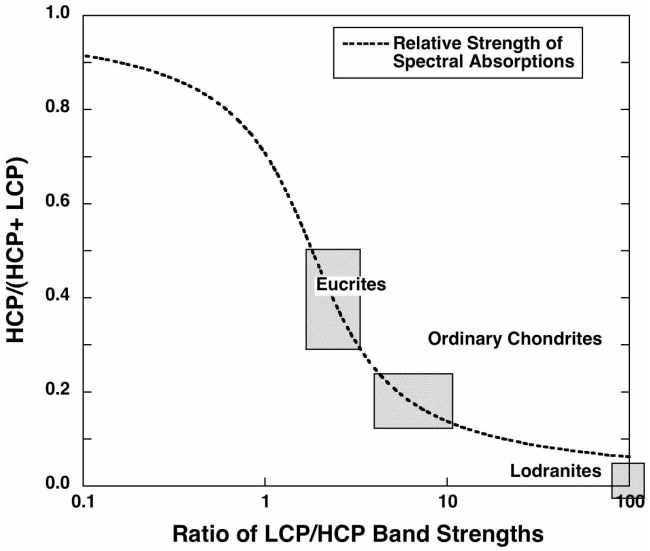

Fig. 2. Systematic variation in the relative strength of pyroxene absorptions as a function of HCP/(HCP + LCP) ratios. Sunshine and Pieters (1993) derived the relationship from spectra of a suite of powders of known proportions of high- and low-calcium pyroxene. As indicated, the relationship can be used to separate meteorite classes that have undergone various degrees of igneous processing (see Fig. 1).

METHODS

Collection and Reduction of Asteroid Spectra

As part of an on-going survey of silicate-rich asteroids (Bus et al. 2001), many high quality near-infrared spectra have been obtained using SpeX at the NASA Infrared Telescope Facility (IRTF) on Mauna Kea. The goal of this program is to sample the full range of silicate mineralogies present among the main-belt asteroids and to map out the distribution of these mineralogies as a function of location across the main-belt. Our initial focus has been on observing members of S-type asteroid families. These families form through collisional processes, and allow us to search for spectral variations among the fragments of once larger parent bodies. Because of this early focus of our survey, however, the initial data set is heavily biased in favor of silicate-rich asteroid family members.

SpeX is a low- to medium-resolution near-infrared spectrograph and imager that uses a pair of InSb array detectors (Rayner et al. 2003). In its low-resolution prism mode, SpeX is capable of recording the wavelength interval from 0.8 to 2.5 μm in a single exposure with a dispersion of ~0.0035 μm per pixel. Our observations were made using a slit width of 0.8 arc-seconds, resulting in a spectral resolution of R ~100. Exposures (with maximum integration times of 120 sec) were taken in pairs in which the location of the spectral image was alternated between "A-beam" and "B-beam" positions by nodding the telescope along the length of the slit. These image pairs provide near-simultaneous measurements of the sky background that were subtracted as part of the data reduction process. Each asteroid observation included several A-B pairs of images that were later combined to obtain the desired signal-to-noise level. Every night, a set of 3 to 5 solar-like stars were also observed, along

with flat-field and Ar-lamp images that were used in calibrating the asteroid spectra.

The steps used in extracting and calibrating the near-infrared asteroid spectra are similar to those used to reduce visible-wavelength CCD spectra. First, a flat-field correction is applied to each image. Then, the complementary images from each A-B pair are subtracted, producing a positive-negative pair of spectra on each image, in which the background level is approximately zero. To achieve the highest possible signal-to-noise ratio, all of the positive spectral images for each asteroid or star are then shifted, scaled, and averaged into a single 2-D spectral image. Discrepant (hot) pixels are rejected during this step using a robust mean.

Extraction of the 1-D spectrum consists of tracing the peak flux along the length of the averaged spectral image and defining an aperture of fixed width that was centered along this trace. Each column of pixels contained within this aperture is then summed. Any residual sky values that may not have been removed as part of the A-B or B-A subtractions are fitted along the pixel columns outside of the aperture and are subtracted as part of this extraction. Using the positions of emission lines contained in the Ar-lamp images, a dispersion function is generated so that accurate wavelength values can be attached to each extracted 1-D spectrum.

The averaged asteroid spectrum is then divided by that of a solar-like star, producing a relative reflectance spectrum for the asteroid. To minimize the uncertainties in our reduced spectra that may result from our choice of solar-like stars, we have limited our calibrations to a set of 13 G-type stars that are spaced around the sky. Two of these stars, 16 CygB and Hyades 64, are accepted as being good solar analogues at visible wavelengths, and the remaining 11 stars appear to be spectrally equivalent to these two analogues in the near-infrared. To reduce any uncertainties tied to the use of a single solar-like star, the asteroid spectrum is normalized to each of the solar standards observed on that night, and the results are averaged.

The presence of strong atmospheric absorption bands, due to H_2O and CO_2, necessitates an extra component in the normalization process. Rapid fluctuations in the amount of precipitable water vapor above the observing location and differences in airmass through which the observations are made can lead to large variations in the depths of these absorption bands. We model the atmospheric transmission using the ATRAN software package (Lord 1992) and fit for the instantaneous amount of precipitable water, allowing us to correct for the telluric features in both the asteroid and standard star spectra as part of the final calibration process.

To produce the final spectra, each near-infrared reflectance spectrum is scaled to match a visible spectrum (already normalized to unity at 0.55 μm) from SMASS (Small Main-Belt Asteroid Spectroscopic Survey; Xu et al. 1995; Bus and Binzel 2002) using the region between 0.82 and 0.92 μm where the visible and near-infrared spectra overlap. The observational parameters for asteroid spectra used in this study are given in Table 1.

Sample Preparation and Data Collection of Meteorite Spectra

To verify our spectral analysis methods, we analyzed two meteorites that represent example end members of igneous differentiation: a basaltic eucrite, Bouvante (Burbine et al. 2001a), and a residual from melting, the primitive achondrite Lodran (Burbine et al. 2001b). Lodran, which includes no plagioclase, contains 37% olivine, 36% low-calcium pyroxene, ~1% high-calcium pyroxene, 25% metallic iron, and 1% chromite (Prinz et al. 1978; Mori et al. 1984). Delaney et al. (1984a) reported modal analyses for the Bouvante basaltic eucrite of 9% orthopyroxene, 24% "pigeonite," 15% augite, 45% plagioclase, and 6% silica. Their "pigeonite" component appears to include both true pigeonite ($Wo_{5–15}$) and submicron-scale mixtures of low-calcium pyroxene and augite as measured by the electron microprobe. Even if we lump their orthopyroxene and pigeonite as low-calcium pyroxene, we still derive a HCP/(HCP + LCP) ratio of ~30%. The actual value is likely to be higher, perhaps 40–50%.

Bouvante and Lodran were both ground in an agate mortar. Bouvante was sieved to a grain size of less than 25 μm, and Lodran was sieved to a grain size of less than 125 μm. (It should be noted that the Lodran sample is depleted in metal relative to the bulk meteorite due to the problems of grinding metallic iron.) Reflectance spectra were obtained using the bi-directional spectrometer at Brown University's Keck/NASA Reflectance Experiment Laboratory (RELAB; Pieters and Hiroi 2004). The spectral coverage was 0.32 to 2.55 μm. The data were collected at a spectral resolution of 5 nm for Bouvante and 10 nm for Lodran. Both spectra were measured at an incident angle of 30° and emission angle of 0°.

RESULTS

High-Calcium Pyroxene in Differentiated Meteorites: Testing MGM

To build confidence in our results and to provide a basis for comparison to asteroid spectra, we first examine the spectra of the primitive achondrite Lodran and the Bouvante eucrite. The MGM fit to Lodran is shown in Fig. 3a. Based on visual inspection, it is clear that the spectrum of Lodran has both pyroxene and olivine components (broad 1 μm and clear 2 μm features). However, there are a number of olivine and pyroxene absorptions in the 1 μm region, which presents an added challenge for absorption band modeling. Even one pyroxene and one olivine require four absorption bands, each with three parameters (center, width, strength), for 12 free parameters in the 1 μm region. Previous work has shown that

Table 1. Observational details for asteroid spectra presented in this paper.

Asteroid	Family	Spectral range	UT date	Exposure (sec)	Mean airmass	Prec. water (mm)[a]	Helio. dist. (AU)	Phase angle (deg)	V mag.
17 Thetis	N/A	Vis[b]	21 Aug 1993	200	1.17		2.47	18.1	11.8
		NIR[c]	15 Aug 2001	630	1.03	1.6	2.59	22.6	12.6
808 Merxia	Merxia	Vis	13 May 1995	1200	1.46		3.00	3.1	13.9
		Vis	06 Sep 1996	1200	1.44		2.97	11.1	14.4
		Vis	08 Sep 1996	1200	1.44		2.97	11.8	14.4
		NIR	14 Aug 2001	1680	1.05	1.4	2.81	13.3	14.2
847 Agnia	Agnia	Vis	15 Nov 1994	1200	1.05		2.57	21.8	15.0
		Vis	29 Jan 1996	1200	1.28		2.67	10.5	14.3
		NIR	19 Feb 2001	600	1.01	1.0	2.82	4.3	14.3
1020 Arcadia	Agnia	Vis	30 Mar 1994	1800	1.18		2.69	4.4	15.6
		NIR	17 Mar 2003	1920	1.01	1.2	2.74	12.2	16.2
1228 Scabiosa	Agnia	Vis	12 Sep 1996	1800	1.02		2.82	19.5	16.5
		NIR	16 Mar 2003	1920	1.21	0.6	2.69	10.9	15.6
1662 Hoffmann	Merxia	Vis	09 May 1995	1800	1.99		2.96	16.5	16.3
		NIR	17 Mar 2003	2400	1.19	1.2	3.18	8.1	16.2
2042 Sitarski	Merxia	Vis	10 May 1995	1800	1.76		3.14	2.2	17.2
		NIR	23 Aug 2001	1920	1.18	2.1	2.68	8.6	16.7
2401 Aehlita	Agnia	Vis	08 Feb 1995	1800	1.02		2.60	20.5	16.9
		NIR	17 Aug 2002	1920	1.44	5.6	2.88	5.9	16.4
2504 Gaviola	Merxia	Vis	15 Oct 1996	1800	1.11		2.97	2.7	16.2
		NIR	17 Aug 2003	2400	1.09	1.2	2.53	20.7	16.5
3363 Bowen	Merxia	Vis	14 Dec 1995	1800	1.10		2.69	12.4	16.2
		NIR	15 Apr 2002	2880	1.19	1.0	2.70	4.9	15.7
3395 Jitka	Agnia	Vis	14 Dec 1995	1800	1.08		2.64	8.7	15.6
		NIR	19 Feb 2001	1680	1.02	1.0	2.66	5.6	15.4
4188 Kitezh	Vesta	Vis	08 Feb 1996	1800	1.16		2.55	0.4	15.8
		NIR	14 Aug 2001	1680	1.29	1.5	2.10	10.8	15.3

[a]Amounts of precipitable water above Mauna Kea was determined from fits to telluric water bands in the SpeX data using the ATRAN model (Lord 1992).
[b]Visible CCD spectra cover 0.44 to 0.92 μm and were taken with MDM Observatory 2.4-m Hiltner Telescope.
[c]Near-infrared SpeX spectra cover 0.82 to 2.49 μm and were taken with 3.0-m NSAS IRTF on Mauna Kea.

with so many degrees of freedom, unconstrained modeling of pyroxene-olivine mixtures results in physically unrealistic solutions (Sunshine 1997). In modeling the spectrum of Lodran, we, therefore, constrain the band parameters of the three olivines absorptions to be consistent with their known values and compositional variations (Sunshine et al. 1998). As in these previous studies (Sunshine 1997; Sunshine et al. 1998), our starting model for olivine absorptions is consistent with an intermediate Fe-Mg composition olivine. Strong correlations are added to the band centers (correlation coefficient of 0.9) so that the band centers shift together as predicted by crystal field theory (Burns 1993) and confirmed with well-characterized laboratory samples (Sunshine and Pieters 1998). Similarly, widths are allowed to vary with the range observed in olivine separates. Finally, the relative band strengths are constrained to be consistent with a Mg-rich olivine. It is important to note that none of these constraints is rigid. Instead, they are added with uncertainties and balanced with minimizing the error in reproducing the measured spectra.

From this modeling, we find that the spectrum of Lodran is best fit by a mixture of low-calcium pyroxene and olivine (see Fig. 3a). There is no evidence for additional components. In particular, there is no evidence for high-calcium pyroxene. The lack of spectrally detectable high-calcium pyroxene is consistent with Lodran's origin as a primitive achondrite with HCP/(HCP + LCP) <10% (see Figs. 1 and 2).

The MGM fit to the Bouvante basaltic eucrite (Fig. 3b) indicates the presence of both low- and high-calcium pyroxene but does not require olivine to fit the overall spectrum. These absorption band modeling results are consistent with the known composition of Bouvante. Based on the relative strength of LCP/HCP absorptions, we derive HCP/(HCP + LCP) of 0.29 (from 1 μm bands ratios) to 0.42 (from 2 μm band ratios). These agree favorably with the electron microprobe modal analyses of (Christophe Michel-Levy et al. 1987), which determined the HCP/(HCP + LCP) ratio for Bouvante to be 0.32. Petrologically, Bouvante is known to lack olivine. As noted previously, both plagioclase and high-calcium pyroxene have absorptions near 1.2 μm.

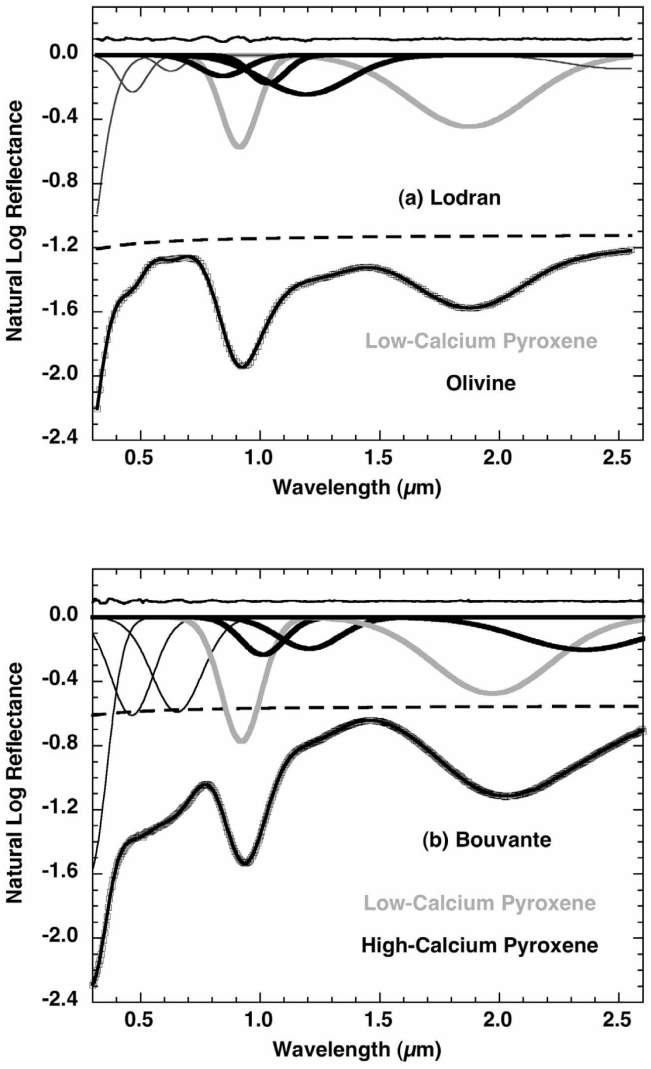

Fig. 3. Absorption band models of the spectra of (a) Lodran, a primitive achondrite, and (b) Bouvante, a basaltic eucrite. In both figures, measured spectra are shown in points, overlain by the modeled spectrum. The residual error between the model and the measured spectrum is displayed at the top of each plot (offset 10% for clarity). The model consists of absorption bands superimposed on the baseline continuum (dashed line). For Lodran, absorption bands from both low-calcium pyroxene (grey) and olivine (thick black) are modeled. For Bouvante, both low-calcium (grey) and high-calcium (thick black) pyroxene absorptions are modeled.

Given this ambiguity between the M1 absorption band in high-calcium pyroxene and the only diagnostic absorption in plagioclase, it is difficult to infer plagioclase content in the presence of high-calcium pyroxene. Nonetheless, the absorption centered near 1.2 μm is relatively strong compared to the primary high-calcium absorption band (near 1.0 μm), suggesting a relatively high proportion of plagioclase, consistent with the basaltic mineralogy of Bouvante (45% plagioclase). These results suggest that the MGM technique can be used to effectively infer the mineralogy of the Bouvante eucrite.

HCP-Rich Asteroids

847 Agnia, 808 Merxia, and 17 Thetis

Bolstered by our success in modeling laboratory spectra of differentiated meteorites, we now turn our attention to applying the MGM technique to asteroid spectra. Among the first set of SpeX asteroid data, we found several asteroids that appeared to be pyroxene-rich. MGM modeling of these asteroids (847 Agnia, 808 Merxia, and 17 Thetis) began by modeling them with a single pyroxene. For example, modeling 847 Agnia with a single pyroxene (Fig. 4) results in a solution with high residual errors, particularly in the 2 μm region. A second pyroxene was added to the absorption band model to reduce the error in the 2 μm region.

As shown in Fig. 5a, this two pyroxene model results in an acceptable fit to the spectrum of 847 Agnia, suggesting a surface mixture of both low- and high-calcium pyroxene. The result is similar to that obtained for the Bouvante eucrite. As with Bouvante, interpretation of the absorption band near 1.25 μm is ambiguous, and it could represent an absorption band from the M1 crystallographic site in high-calcium pyroxene and/or from plagioclase. Given the quality of the fit, no additional phases—notably olivine—are required. A lack of olivine is supported by the position of the resultant pyroxene band centers, which lie on the pyroxene trend defined by Adams (1974). Previous workers (e.g., Gaffey et al. 1993) have shown that olivine shifts the apparent pyroxene band centers off this trend. We conservatively place an upper bound of <20% on the abundance of olivine on the surface of 847 Agnia.

Virtually equivalent results were found in modeling the spectra of 808 Merxia and 17 Thetis (Figs. 5b and 5c), indicating that these asteroids have nearly identical surface compositions. The only significant difference among these spectra is in the absolute strengths of the absorption bands, with 17 Thetis having the weakest bands. Based on the ratio of their LCP/HCP band strengths (Fig. 2), all three asteroids have HCP/(HCP + LCP) ratios of ~0.4–0.6 (see Table 2). Among the meteorites, such compositions are most similar to the basaltic achondrites, e.g., the Bouvante eucrite (Fig. 3b).

Interestingly, 17 Thetis, for example, plots in the S(VI) field in the Gaffey et al. classification (Gaffey et al. 1993), which is interpreted to be rich in low-calcium pyroxene with a significant olivine component. Yet, our results indicate an absence of olivine and, instead, a significant component of high-calcium pyroxene. Furthermore, although visual comparison and absorption band modeling of all three asteroids show them to be spectrally very similar, they each plot in very different regions of the Gaffey et al. (1993) band area-band center classification scheme. As such, we, like Gaffey (1993; 2003), caution against the blind use of band area ratios (Cloutis et al. 1986), particularly in the possible presence of high-calcium pyroxene.

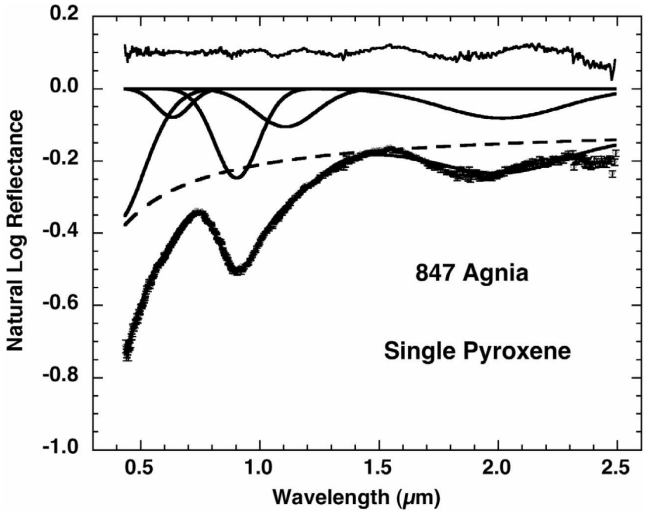

Fig. 4. Absorption band model of the spectrum of 847 Agnia using a single pyroxene. Note the high residual error in the 2 μm region and a similar systematic error in the 1 μm region. This misfit indicates the presence of a second pyroxene. (Curves as in Fig. 3.)

Vestoid: 4188 Kitezh

Given the compositional similarity of these high-calcium pyroxene rich asteroids to Bouvante, a comparison to other HED-like asteroids is warranted. In particular, it has long been argued, based on spectral similarity and favorable dynamics, that 4 Vesta and a series of related objects (the Vestoids) are likely sources of the HED meteorites (e.g., Binzel and Xu 1993). To directly compare our HCP-rich S-type asteroids, we also examine the spectrum of 4188 Kitezh, a Vestoid. As with the Bouvante eucrite and our other asteroids, we find that 4188 Kitezh is well-modeled with absorption bands due to both high- and low-calcium pyroxenes (Fig. 5d). Based on the relative strength of the HCP and LCP absorptions, we infer a HCP/(HCP + LCP) ratio of .3–.4, which is consistent with the known values for Bouvante (see Table 2). Here again, we find no evidence for olivine but infer a plagioclase component. There are minor differences in absorption band parameters (most notably in absolute strength) and differences in continuum slope. Yet, based on the general similarity of their absorption bands, the Bouvante

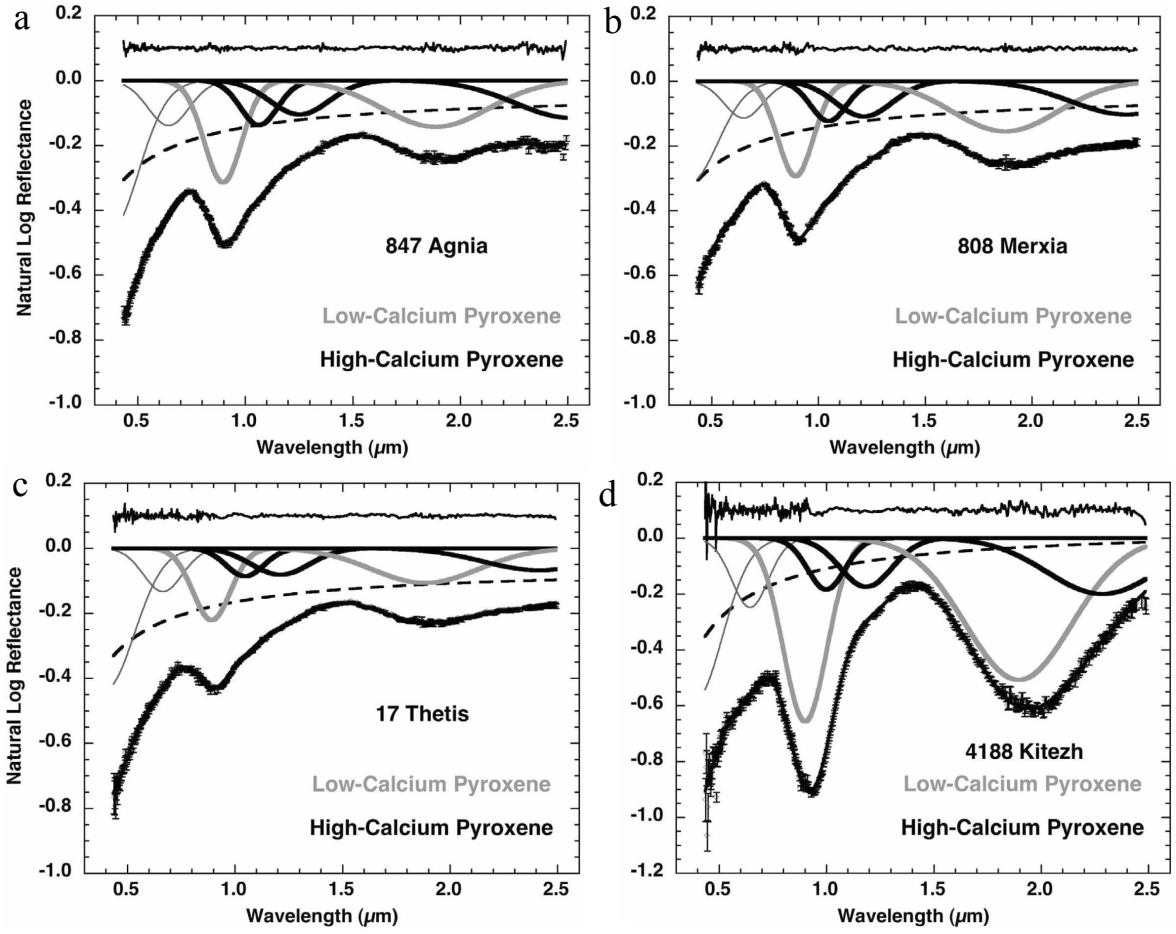

Fig. 5. Absorption band models of 847 Agnia, 808 Merxia, 17 Thetis, and 4188 Kitezh. Each of these spectra includes both low-calcium (grey) and high-calcium (thick black) pyroxene absorptions. (Curves as in Fig. 3.) Although they differ in absolute strength, based on the relative strength of pyroxene absorptions (Fig. 2), we infer that each of these asteroids have high-calcium pyroxene to total pyroxene ratios of ~0.4 and, thus, are broadly basaltic surfaces.

Table 2. Absorption band parameters for spectra modeled in this work.

	Center (nm)	FWHM (nm)[a]	Strength (log reflectance)	Str. LCP/Str. HCP[b]	HCP/(HCP + LCP)[c]	Continuum/ Error in fit[d]
Lodran						
Band 1	174	248	–2.58			
Band 2	466	139	–0.23			
Band 3	627	127	–0.10			
Band 4	913	178	–0.57			Offset
Band 5	1874	585	–0.45			.33
Band 6	2500	507	–0.08			Slope
Band 7	845	228	–0.13			–9.5E-07
Band 8	1033	176	–0.18			Error
Band 9	1193	424	–0.24			0.52%
Bouvante eucrite						
Band 1	287	169	–1.60			
Band 2	464	206	–0.61			
Band 3	652	244	–0.59			Offset
Band 4	922	198	–0.77	3.3	0.29	0.58
Band 5	1011	213	–0.23			Slope
Band 6	1205	304	–0.20			–1.06E-06
Band 7	1971	574	–0.48	2.3	0.42	Error
Band 8	2355	622	–0.20			0.39%
847 Agnia-single pyroxene						Offset
Band 1	384	304	–0.38			.91
Band 2	636	166	–0.08			Slope
Band 3	903	218	–0.25			–9.50E-06
Band 4	1108	299	–0.11			Error
Band 5	2016	603	–0.08			1.21%
847 Agnia						
Band 1	369	317	–0.47			
Band 2	644	226	–0.14			Offset
Band 3	897	204	–0.31	2.3	0.40	.96
Band 4	1064	204	–0.14			Slope
Band 5	1252	319	–0.10			–9.98E-06
Band 6	1884	576	–0.14	1.2	0.64	Error
Band 7	2516	608	–0.12			0.57%
808 Merxia						
Band 1	395	316	–0.31			
Band 2	649	214	–0.11			Offset
Band 3	893	197	–0.29	2.4	0.39	.97
Band 4	1048	200	–0.12			Slope
Band 5	1213	311	–0.11			–1.00E-05
Band 6	1874	579	–0.16	1.5	0.58	Error
Band 7	2442	608	–0.10			0.56%
17 Thetis						
Band 1	397	319	–0.43			
Band 2	665	214	–0.13			Offset
Band 3	892	206	–0.22	2.6	0.37	.95
Band 4	1046	206	–0.09			Slope
Band 5	1211	315	–0.08			–9.9E-06
Band 6	1882	579	–0.11	1.6	0.55	Error
Band 7	2414	610	–0.07			0.62%
4188 Kitezh						
Band 1	384	308	–0.58			Offset
Band 2	644	201	–0.25			1.05
Band 3	901	239	–0.66	3.6	0.27	Slope

Table 2. Absorption band parameters for spectra modeled in this work. *Continued.*

	Center (nm)	FWHM (nm)[a]	Strength (log reflectance)	Str. LCP/Str. HCP[b]	HCP/(HCP + LCP)[c]	Continuum/ Error in fit[d]
Band 4	999	205	–0.18			–1.49E-05
Band 5	1185	285	–0.17			Error
Band 6	1895	585	–0.51	2.5	0.39	1.89%
Band 7	2284	604	–0.20			Offset

[a]Full width at half maximum.
[b]Strength of high-calcium absorption/strength of low-calcium absorption.
[c]Inferred from relationship in Fig. 2.
[d]Continuum parameters (slope and offset in energy).

eucrite and all the asteroids studied here (including the high-calcium-rich S-type asteroids and the Vestoid 4188) have similar mafic silicate mineralogies.

DISCUSSION

Evidence for Differentiation

In this work, we have examined three S-type asteroids that are best explained as mixtures of high-calcium pyroxene, low-calcium pyroxene, and plagioclase, with relatively minor amounts of olivine. The olivine and plagioclase abundances are difficult to derive, but we estimate no more than 20% olivine. In contrast, it is relatively simple to derive HCP/(HCP + LCP) ratios, and we arrive at values of ~0.4–.6 for our HCP-rich asteroids (847 Agnia, 808 Merxia, and 17 Thetis). These values are clearly inconsistent with any known chondritic material. Ordinary chondrites exhibit HCP/(HCP + LCP) ratios of ~0.1–0.2 and are typically dominated by olivine (McSween et al. 1991). The enstatite chondrites are rich in low-calcium pyroxene, with minor amounts of olivine and high-calcium pyroxene (a few percent) in type 3 enstatite chondrites (Brearley and Jones 1998). However, enstatite chondrites are essentially FeO-free (Keil 1968) and do not exhibit spectral absorption features seen in these asteroids. The high HCP/(HCP + LCP) ratios derived here require relatively extensive differentiation of these asteroids and/or their primordial parent asteroid. Obtaining HCP/(HCP + LCP) ratios greater than 0.3 requires less than ~30% partial melting of an ordinary chondrite precursor (Fig. 1). This is comparable to the degree of melting that produced the eucrites, suggesting a comparable geologic history for these asteroids and/or their parent asteroid and the putative parent body of the eucrites, 4 Vesta.

Although broadly similar, there are differences between the HCP-rich asteroids and eucrites. Compared to Bouvante, the HCP-rich asteroids have a higher percentage of their pyroxene as high-calcium pyroxene. Higher HCP/(HCP + LCP) ratios typically indicate earlier partial melts (Fig. 1). While it is tempting to interpret the HCP-rich S-type asteroids as sampling lower degrees of partial melting, we caution that these hemispherically averaged asteroid spectra represent mixtures of evolved igneous lithologies, including basalts, cumulate orthopyroxenites, and, perhaps, dunites extracted from the lower crust or mantle. To test this hypothesis, we examined the SpeX spectra of several members of both the Agnia and Merxia families (Fig. 6). Detailed comparison among and between these families will be the subject of a future paper. However, it is clear even from visual examination of the data that there is no evidence for significant compositional heterogeneity within either family.

The recognition of three additional asteroids/asteroid families that experienced extensive melting and differentiation more than doubles our inventory of such asteroids. Prior to this work, only 4 Vesta (and the Vestoids) and 1459 Magnya (Lazzaro et al. 2000; Michtchenko et al. 2002; Hardersen et al. 2004) and a few near-Earth asteroids (Cruikshank et al. 1991; Binzel et al. 2001) were believed to have basaltic surface mineralogies. It is actually gratifying that we are recognizing an increasing number of differentiated asteroids. The meteorite record suggests that we have sampled ~100–150 meteorite parent bodies, of which ~27 are chondritic (Wasson 1990; Meibom and Clark 1999; Burbine et al. 2003). Thus, most of the asteroids delivering meteorites to Earth are probably differentiated.

Spectral Differences between Merxia/Agnia and Vestoids/Eucrites

Even though 4 Vesta/Vestoids and the HCP-rich S-type asteroids such as Thetis, Agnia, and Merxia have similar interpreted silicate mineralogies, visually their spectra appear different. Most noticeably, 4 Vesta/Vestoids have much deeper band depths than the HCP-rich S-type asteroids. The spectra of 4 Vesta/Vestoids much more closely resemble the HEDs than the HCP-rich S-type asteroids. There are several possible explanations for the differences between the HCP-rich asteroids, Vesta, the Vestoids, and eucrites.

One possibility is that the HCP-rich S-type asteroids have a higher abundance of opaque minerals (e.g., metallic iron, troilite, magnetite, carbon) than 4 Vesta/Vestoids. These minerals have similar spectral effects when admixed, reducing the albedo of the mixture and the depths of any absorption bands (e.g., Cloutis et al. 1990a, b). The concentration of opaques needed to reduce band depths is a function of particle size. Adding only 0.5 wt% of very fine-

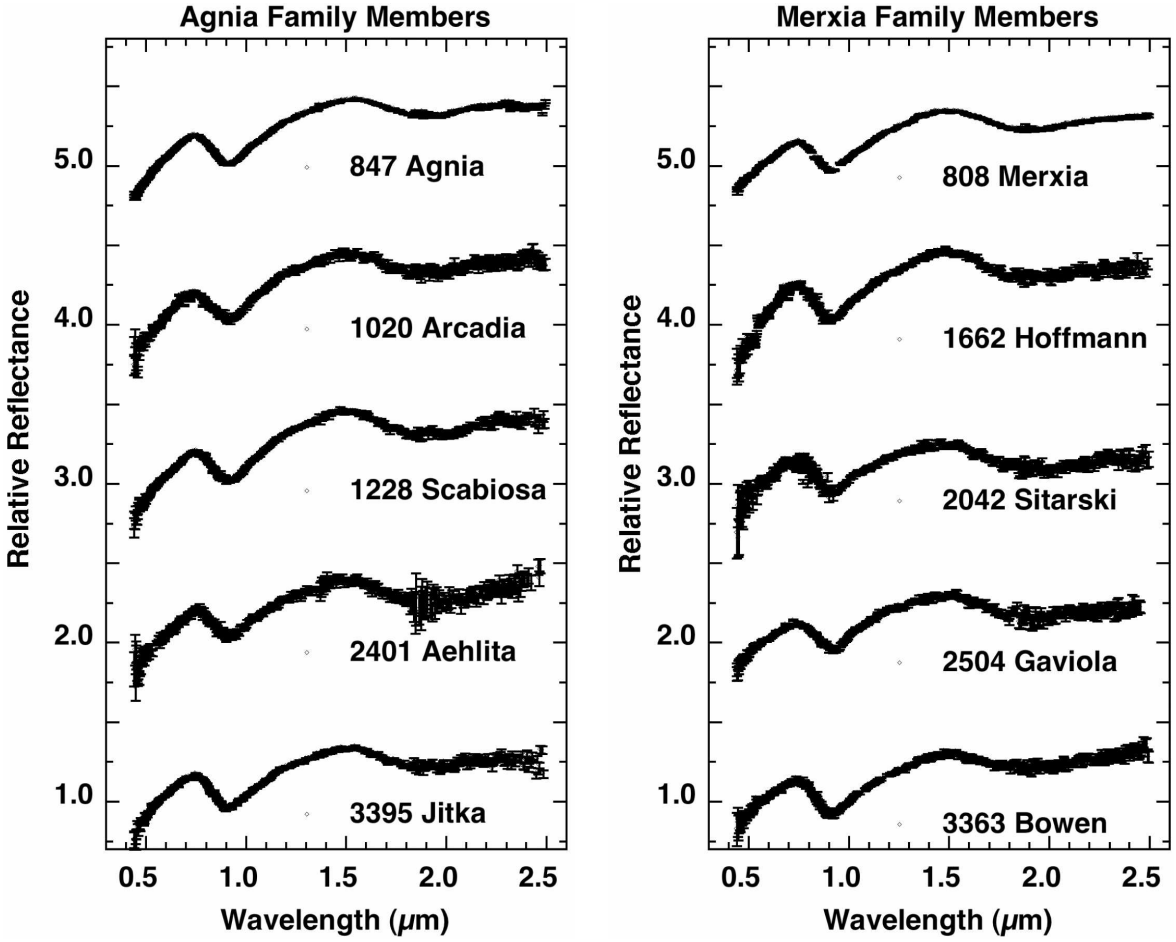

Fig. 6. Visible and near-infrared spectra of Agnia and Merxia family members measured to date. As indicated in Table 1, many of these smaller objects have V magnitudes >15.5 yet have high SNR. Note the spectral similarity within and between these two families.

grained carbon (<0.023 micron) significantly reduces the band depth of a pyroxene mixture (Cloutis et al. 1990b). Larger percentages (~25 wt%) of larger (45–90 μm) grains of metallic iron are needed for similar effects on a pyroxene mixture (Cloutis et al. 1990a).

HEDs do contain carbonaceous chondrite clasts (e.g., Zolensky et al. 1996; Buchanan and Mittlefehldt 2003) but typically in very small concentrations (<1%). Recent observations of 4 Vesta (Hasegawa et al., 2003) show a weak (at the 1% level) 3 μm absorption feature that may be indicative of carbonaceous chondritic material on its surface. Although unlikely, the spectral difference between 4 Vesta/Vestoids and the HCP-rich asteroids might suggest a higher abundance of carbonaceous chondritic material accreted to the latter, reducing the absorption feature band depths.

Opaque minerals are also relatively rare in HED meteorites. However, the mesosiderites, which are mixtures of basaltic, gabbroic, and pyroxenitic lithologies with metallic iron, contain between 20 and 90% opaque phases (metallic iron and troilite) (Mittlefehldt et al. 1998). Mesosiderites are metal-pyroxene-rich assemblages, while most other metal-silicate-rich achondrites contain abundant olivine. Thus, although the exact mechanism by which the mesosiderites formed is unknown, it is possible that the HCP-rich S-type asteroids are more akin to the mesosiderite parent body than the eucrite parent body.

Finally, submicroscopic iron is thought to be concentrated on asteroid surfaces as a product of "space weathering" processes (e.g., Pieters et al. 2000; Hapke 2001; Clark et al. 2003). If the HCP-rich S-type asteroids have more Fe-rich opaques than 4 Vesta/Vestoids, this might enhance the production of submicroscopic iron. Sasaki et al. (2001) were able to duplicate space weathering effects in the laboratory using a pulsed laser to mimic the energy of micrometeorite impacts and produce vapor-deposited submicroscopic iron grains on irradiated olivine samples. These submicroscopic iron grains appear much easier to produce on irradiated olivine samples than pyroxene ones (Yamada et al. 1999). Higher abundances of submicroscopic iron in the HCP-rich S-type asteroids could, therefore, imply that these objects have higher abundances of olivine than 4 Vesta/Vestoids and, thus, have surfaces that are more conducive to producing submicroscopic iron. However, the HCP-rich S-type asteroids

all have relatively small amounts of olivine (<20%). Thus, it is more likely that higher abundances of submicroscopic iron in the HCP-rich S-type asteroids compared to 4 Vesta/Vestoids would imply older, more "space weathered," surfaces on the HCP-rich S-asteroids.

Implications for Asteroid Families

The initial set of HCP-rich S-type asteroids presented here includes two families, Merxia and Agnia. We have found that the largest members in the Merxia and Agnia family members are mineralogically "identical." They all contain two pyroxenes with high HCP/(HCP + LCP) ratios and plagioclase. This suggests a homogenized family with a broadly "basaltic" surface. These results indicate that the family members retain no evidence of significant lateral heterogeneities in the pre-family forming asteroids.

Based on these observations, we also find no evidence of vertical heterogeneities among either the Agnia or Merxia families. Similarly, existing data for 4 Vesta/Vestoids (including extensive visible spectra and limited infrared-data) have identified only basaltic surfaces. Thus, none of these three evolved families corresponds to the simple geologically stratified model (basaltic crust, mantle, core) that has been often proposed as the typical model for the igneous asteroid family (Gaffey et al. 2003). Based on these results, we caution against using the stratified model to search for, or as the only evidence for, igneous families. Instead, we suggest that the most reasonable explanation for the homogeneity of the Agnia and Merxia families is that both are secondary families formed from the breakup of a basaltic fragment from a primary asteroid parent body. Alternatively, the Agnia and Merxia families could be primary families formed from the breakup of basaltic bodies with lateral heterogeneity smaller than the scale of any of the family members. It is also possible that these asteroids have experienced an impact history that has homogenized their surfaces. The family forming process itself may have homogenized the original body, which then re-accumulated into family members, as suggested by Michel et al. (2001).

Future Efforts

We have identified spectra of several asteroids from our initial set of SpeX data that are dominated by absorptions from two phases of pyroxene. With some ambiguity, we have also inferred that these objects contain significant plagioclase. In future studies, we must build models to more rigorously quantify the modal abundances of pyroxene and plagioclase.

Previous studies (McSween et al. 1991; Gaffey and Gilbert 1998) have shown that high-calcium pyroxene is also present in ordinary chondrites. In addition, high-calcium pyroxene was inferred (although not unambiguously detected) in analyses of NEAR-Shoemaker spectra of Eros (McFadden et al. 2001). Based on our work, we now recognize that quantifying the relative proportions of high-calcium pyroxene is not only possible with high-quality SpeX data, but also that it is a sensitive indicator of igneous history. In addition, preliminary modeling of spectra of silicates from ordinary chondrites (Sunshine et al. 2002) has shown that their spectra unambiguously require olivine, low-calcium pyroxene, and high-calcium pyroxene absorptions. Furthermore, the modes and compositions inferred for these meteorite spectra are consistent with known petrography. Thus, the methods we have used in the research presented here, when expanded to ternary mixtures, hold great promise for directly detecting and quantify the presence of high-calcium pyroxene in silicate-rich asteroid spectra.

CONCLUSIONS

We study asteroids and their meteoritic samples to understand their petrogenetic history, including both solar nebular processes and later asteroid differentiation. We have demonstrated that HCP/(HCP + LCP) ratios provide an excellent measure of differentiation and can be readily determined by our Modified Gaussian Method technique. HCP/(HCP + LCP) ratios are in the range of 0.1–0.2 in primitive chondritic meteorites, while differentiated meteorites and their asteroidal sources have either little HCP in residual melts (e.g., primitive achondrites) or high concentration of HCP crystallized from partial melts (e.g., basaltic achondrites). Asteroids with high (>0.3) HCP/(HCP + LCP) ratios are not uncommon in the asteroid belt. In addition to the well-known Vestoids, we find similarly high ratios in the members of two asteroid families (Merxia, Agnia) and one non-family asteroid (Thetis). In addition to the high HCP/(HCP + LCP) ratios, these asteroids all appear to contain abundant plagioclase and minor amounts of olivine, although these abundances are more difficult to quantify. This common silicate mineralogy is inconsistent with all known chondrites and is best explained as the result of partial melting of a chondritic precursor. Eucritic meteorites, which are derived from such a partial melt, share this silicate mineralogy, implying a similar petrogenesis operating on multiple parent bodies. The widespread nature of this mineralogy is not unexpected, given the evidence for numerous differentiated parent bodies in the meteorite record. Despite their common derived mineralogy and petrogenesis, the asteroids discussed here differ in their overall spectral slope and band strength. We attribute this difference to the addition of metal, either through space weathering and production of nanophase iron or admixture of larger metal particles like those found in mesosiderites. The similar mineralogy that dominates both the Merxia and Agnia families suggests that all members experienced nearly identical histories, possibly when these families formed by the breakup of a basaltic fragment of a previously destroyed

proto-asteroid. Finally, we suggest that the approach taken to identify the mineralogy of these asteroids and their HCP/(HCP + LCP) ratios might also provide a tool for discovering ordinary chondritic asteroids.

Acknowledgments–Support for this research from NASA's PGG program (NASW-00012 to J. M. Sunshine), NSF (AST-0307688 to S. J. Bus), NASA's Cosmochemistry Program (NAG5–13464 to T. J. McCoy and C. M. Corrigan), and the Becker Endowment to the Smithsonian Institution is greatly appreciated. All meteorite spectra were collected at Brown University's Keck/NASA Reflectance Experiment Laboratory (RELAB), a multi-user facility supported by NASA (NAG5–13609). We are grateful to E. Cloutis and T. Hirori for carefully considered reviews that strengthened this manuscript.

Editorial Handling—Dr. Beth-Ellen Clark

REFERENCES

Adams J. B. 1968. Lunar and martian surfaces: Petrologic significance of absorptions bands in the near-infrared. *Science* 159:1453–1455.

Adams J. B. 1974. Visible and near-infrared diffuse reflectance spectra of pyroxene as applied to remote sensing of solid objects in the solar system. *Journal of Geophysical Research* 79:4829–4836.

Asimow P. D. and Ghiorso M. S. 1998. Algorithmic modifications extending MELTS to calculate sub-solidus phase relations. *American Mineralogist* 83:1127.

Binzel R. P. and Xu S. 1993. Chips off of asteroid 4 Vesta: Evidence for the parent body of basaltic achondrite meteorites. *Science* 260:186.

Binzel R. P., Harris A. W., Bus S. J., and Burbine T. H. 2001. Spectral properties of near-Earth objects: Palomar and IRTF results for 48 objects including spacecraft targets (9969) Braille and (10302) 1989 ML. *Icarus* 151:139–149.

Brearley A. J. and Jones R. H. 1998. Chondritic meteorites. In *Planetary materials,* edited by Papike J. J. Washington D. C.: Mineralogic Society of America. pp. 3-1–3-398.

Britt D. T., Bell J. F., Haack H., and Scott E. R. D. 1992. The reflectance spectrum of troilite and the T-type asteroids. *Meteoritics* 27:207.

Buchanan P. C. and Mittlefehldt D. W. 2003. Lithic components in the paired howardites EET 87503 and EET 87513: Characterization of the regolith of 4 Vesta. *Antarctic Meteorite Research* 16:128–151.

Burbine T. H., Buchanan P. C., Binzel R. P., Bus S. J., Hiroi T., Hinrichs J. L., Meibom A., and McCoy T. J. 2001a. Vesta, vestoids, and the howardite, eucrite, diogenite group: Relationships and the origin of spectral differences. *Meteoritics & Planetary Science* 36:761–782.

Burbine T. H., McCoy T. J., Nittler L. R., and Bell J. F., III. 2001b. Could 433 Eros have a primitive achondritic composition? (abstract #1860). 32nd Lunar and Planetary Science Conference. CD-ROM.

Burbine T. H., McCoy T. J., Meibom A., Gladman B., and Keil K. 2003. Meteoritic parent bodies: Their number and identification. In *Asteroids III,* edited by Bottke W. F., Jr., Cellino A., Paolicchi P., and Binzel R. P. Tucson: University of Arizona Press. pp. 653–667.

Burns R. G. 1993. *Mineralogical applications of crystal field theory, 2nd edition.* New York: Cambridge University Press. 551 p.

Bus S. J. and Binzel R. P. 2002. Phase II of the small main-belt asteroid spectroscopic survey—The observations. *Icarus* 158: 106–145.

Bus S. J., Sunshine J. M., Binzel R. P., and Burbine T. H. 2001. Investigating asteroids on the olivine-to-pyroxene continuum (abstract). *Bulletin of the American Astronomical Society* 33:118.

Camara F., Doukhan J. C., Domeneghetti M. C., and Zema M. 2000. A TEM study of ca-rich orthopyroxenes with exsolution products: Implications for Mg-Fe ordering process. *European Journal of Mineralogy* 12:735–748.

Christophe Michel-Levy M., Bourot-Denise M., Palme H., Spettel B., and Wänke H. 1987. L'eucrite de bouvante: Chimie, pétrologie, et minérologie. *Bulletin of Mineralogy* 119:449–458.

Clark B. E., Hapke B., Pieters C., and Britt D. 2003. Asteroid space weathering and regolith evolution. In *Asteroids III,* edited by Bottke W. F., Jr., Cellino A., Paolicchi P., and Binzel R. P. Tucson: University of Arizona Press. pp. 585–599.

Cloutis E. A. and Burbine T. H. 1999. The spectral properties of troilite/pyrrhotite and implications for the E-asteroids (abstract). *Lunar and Planetary Institute Conference Abstracts* 30:1875.

Cloutis E. A. and Gaffey M. J. 1991. Pyroxene spectroscopy revisited: Spectral-compositional correlations and relationships to geothermometry. *Journal of Geophysical Research* 96:22809–22826.

Cloutis E. A., Gaffey M. J., Jackowski T. L., and Reed R. L. 1986. Calibrations of phase abundance, composition, and particle size distributions for olivine-orthopyroxene mixtures from reflectance spectra. *Journal of Geophysical Research* 91:11641–11653.

Cloutis E. A., Gaffey M. J., and Smith D. G. W. 1990a. Metal silicate mixtures: Spectral properties and applications to asteroid taxonomy. *Journal of Geophysical Research—Solid Earth and Planets* 95:8323.

Cloutis E. A., Gaffey M. J., and Smith D. G. W. 1990b. Reflectance spectra of mafic silicate-opaque assemblages with applications to meteorite spectra. *Icarus* 84:315.

Cruikshank D. P., Tholen D. J., Hartmann W. K., Bell J. F., and Brown R. H. 1991. Three basaltic earth-approaching asteroids and the source of basaltic meteorites. *Icarus* 89:1–13.

Delaney J. S., O'Neill C., and Prinz M. 1984a. Two magma types in the eucrite Bouvante. 15th Lunar and Planetary Science Conference. pp. 210–211.

Delaney J. S., Prinz M., and Takeda H. 1984b. The polymict eucrites. Proceedings of 15th Lunar Planetary Science Conference. *Journal of Geophysics Research* 89:C251–C288.

Gaffey M. J., Burbine T. H., Piatek J. L., Reed K. L., Chaky D. A., Bell J. F., and Brown R. H. 1993. Mineralogical variations within the S-type asteroid class. *Icarus* 106:573–602.

Gaffey M. J., Cloutis E. A., Kelley M. S., and Reed K. L. 2003. Mineralogy of asteroids. In *Asteroids III,* edited by Bottke W. F., Jr., Cellino A., Paolicchi P., and Binzel R. P. Tucson: University of Arizona Press. pp. 183–204.

Gaffey M. J. and Gilbert S. L. 1998. Asteroid 6 Hebe: The probable parent body of the H-type ordinary chondrites and the IIE iron meteorites. *Meteoritics & Planetary Science* 33:1281–1295.

Ghiorso M. S. and Sack R. O. 1995. Chemical mass transfer in magmatic processes IV. A revised and internally consistent thermodynamic model for the interpolation and extrapolation of liquid-solid equilibria in magmatic systems at elevated temperatures and pressures. *Contributions to Mineralogy and Petrology* 119:197.

Hapke B. 2001. Space weathering from Mercury to the asteroid belt. *Journal of Geophysical Research* 106:10039–10073.

Hardersen P. S., Gaffey M. J., and Abell P. A. 2004. Mineralogy of asteroid 1459 Magnya and implications for its origin. *Icarus* 167: 170–177.

Hasegawa S., Murakawa K., Ishiguro M., Nonaka H., Takato N., Davis C., Ueno M., and Hiroi T. 2003. Evidence of hydrated and/ or hydroxylated minerals on the surface of asteroid 4 Vesta. *Geophysical Research Letters* 30, doi: 10.1029/2003GL018627.

Hawke B. R., Peterson C. A., Blewett D. T., Bussey B. J., Lucey P. G., Taylor G. J., and Spudis P. D. 2003. Distribution and modes of occurrence of lunar anorthosite. *Journal of Geophysical Research* 108, doi: 10.1029/2002JE001890.

Hinrichs J. L. and Lucey P. G. 2002. Temperature-dependent near-infrared spectral properties of minerals, meteorites, and lunar soil. *Icarus* 155:169–180.

Hiroi T. and Sasaki S. 2001. Importance of space weathering simulation products in compositional modeling of asteroids: 349 Dembowska and 446 Asternitas as examples. *Meteoritics & Planetary Science* 36:1587–1596.

Hiroi T. and Takeda H. 1991. Reflectance spectroscopy and mineralogy of primitive achondrites-lodranites. *Proceedings of the NIPR Symposium on Antarctic Meteorites* 4:163–177.

Jarosewich E. 1990. Chemical analyses of meteorites—A compilation of stony and iron meteorite analyses. *Meteoritics* 25: 323–337.

Keil K. 1968. Mineralogical and chemical relationships among enstatite chondrites. *Journal of Geophysical Research* 74:6945–6976.

King T. V. V. and Ridley W. I. 1987. Relation of the spectroscopic reflectance of olivine to mineral chemistry and some remote sensing implications. *Journal of Geophysical Research* 92: 11457–11469.

Kullerud G. 1963. The Fe-N-S system. *Annual Report of the Geophysics Laboratory* 67:4055–4061.

Lazzaro D., Michtchenko T., and Harris A. W. 2000. Discovery of a basaltic asteroid in the outer main belt. *Science* 288:2033.

Lord S. 1992. A new software tool for computing Earth's atmospheric transmission of near- and far-infrared radiation. NASA Technical Memorandum 103957.

Lorimer G. W. and Champness P. E. 1973. Combined electron microscopy and analysis of an orthopyroxene. *American Mineralogist* 58:243–248.

McCord T. B., Adams J. B., and Johnson T. V. 1970. Asteroid Vesta: Spectral reflectivity and compositional implications. *Science* 168:1145–1447.

McCoy T. J., Keil K., Clayton R. N., Mayeda T. K., Bogard D. D., Garrison D. H., Huss G. R., Hutcheon I. D., and Wieler R. 1996. A petrologic, chemical, and isotopic study of Monument Draw and comparison with other acapulcoites: Evidence for formation by incipient partial melting. *Geochimica et Cosmochimica Acta* 60:2681–2708.

McFadden L. A., Wellnitz D. D., Schnaubelt M., Gaffey M. J., Bell J. F., III, Izenberg M., Murchie S., and Chapman C. R. 2001. Mineralogical interpretation of reflectance spectra of Eros from NEAR near-infrared spectrometer low phase flyby. *Meteoritics & Planetary Science* 36:1711–1726.

McSween H. Y., Jr., Bennett M. E., III, and Jarosewich E. 1991. The mineralogy of ordinary chondrites and implications for asteroid spectrophotometry. *Icarus* 90:107–116.

Meibom A. and Clark B. E. 1999. Evidence for the insignificance of ordinary chondritic material in the asteroid belt. *Meteoritics & Planetary Science* 34:7.

Michel P., Benz W., Tanga P., and Richardson D. C. 2001. Collisions and gravitational reaccumulation: Forming asteroid families and satellites. *Science* 294:1696–1699.

Michtchenko T. A., Lazzaro D., FerrazMello S., and Roig F. 2002. Origin of the basaltic asteroid 1459 Magnya: A dynamical and mineralogical study of the outer main belt. *Icarus* 158:343–359.

Mittlefehldt D. W., McCoy T. J., Goodrich C. A., and Kracher A. 1998. Non-chondritic meteorites from asteroidal bodies. In *Planetary materials,* edited by Papike J. J. Washington D. C.: Mineralogical Society of America. pp. 195.

Mori H., Takeda H., Prinz M., and Harlow G. E. 1984. Mineralogical and crystallographic studies of lodranite and primitive achondrite groups bearing on their genetic link. (abstract). 15th Lunar and Planetary Science Conference. pp. 567–568.

Moroz L., Schade U., and Wäsch R. 2000. Reflectance spectra of olivine-othopyroxene-bearing assemblages at decreased temperatures: Implications for remote sensing of asteroids. *Icarus* 147:79–93.

Morse S. A. 1980. *Basalts and phase diagrams.* New York: Springer-Verlag. 493 p.

Mustard J. F. 1992. Chemical analysis of actinolite from reflectance spectra. *American Mineralogist* 77:345–358.

Palme H., Schultz L., Spettel B., Weber H. W., Wänke H. Michel-Levy M. C., and Lorin J. C. 1981. The Acapulco meteorite: Chemistry, mineralogy, and irradiation effects. *Geochimica et Cosmochimica Acta* 45:727–752.

Pieters C. A., Taylor L. A., Noble S. K., Keller L. P., Hapke B., Morris R. V., Allen C. C., McKay D. S., and Wentworth S. 2000. Space weathering on airless bodies: Resolving a mystery with lunar samples. *Meteoritics & Planetary Science* 35:1101-1107.

Pieters C. M. and Hiroi T. 2004. Relab user's manual. http:// www.planetary.brown.edu/relab.

Prinz M. R. K., Harlow G. E., and Hewins R. H. 1978. Petrologic studies bearing on the origin of the Lodran meteorite (abstract). 9th Lunar and Planetary Science Conference. pp. 919–921.

Rayner J. T., Toomey D. W., Onaka P. M., Denault A. J., Stahlberger W. E., Vacca W. D., Cushing M. C., and Wang S. 2003. SpeX: A medium-resolution 0.8–5.5 micron spectrograph and imager for the NASA infrared telescope facility. *Publications of the Astronomical Society of the Pacific* 115:362–382.

Sasaki S., Nakamura K., Hamabe Y., Kurahashi E., and Hiroi T. 2001. Production of iron nanoparticles by laser irradiation in a simulation of lunar-like space weathering. *Nature* 410:555–556.

Schade U. and Wäsch R. 1999. Near-infrared reflectance spectra from bulk samples of the two SNC meteorites Zagami and Nakhla. *Meteoritics & Planetary Science* 34:417–424.

Schade U., Wäsch R., and Moroz L. 2004. Near-infrared reflectance spectroscopy of Ca-rich clinopyroxenes and prospects for remote spectral characterization of planetary surfaces. *Icarus* 168:80–92.

Singer R. B. and Roush T. L. 1985. Effects of temperature on remotely sensed mineral absorption features. *Journal of Geophysical Research* 90:12434–12444.

Sunshine J. M. 1997. Continuing towards a more sophisticated compositional interpretations of silicate-rich lithologies on the surfaces of asteroids. 28th Lunar Planetary Science Conference. pp. 1181–1182.

Sunshine J. M., Bus S. J., Burbine T. H., McCoy T. J., and Binzel R. P. 2002. Unambiguous spectral evidence for high- (and low-) calcium pyroxene in asteroids and meteorites (abstract #1356). 33rd Lunar and Planetary Science Conference. CD-ROM.

Sunshine J. M., Hinrichs J. L., and Lucey P. G. 2000. Temperature dependence of individual absorptions bands in olivine: Implications for inferring compositions of asteroid surfaces from spectra (abstract #1605). 31st Lunar and Planetary Science Conference.

Sunshine J. M., McFadden L. A., and Pieters C. M. 1993. Reflectance spectra of the Elephant Moraine A79001 meteorite: Implications for remote sensing of planetary bodies. *Icarus* 105:79–91.

Sunshine J. M. and Pieters C. M. 1993. Estimating modal abundances from the spectra of natural and laboratory pyroxene mixtures using the Modified Gaussian Model. *Journal of Geophysical Research* 98:9075–9087.

Sunshine J. M. and Pieters C. M. 1998. Determining the composition of olivine from reflectance spectroscopy. *Journal of Geophysical Research* 103:13675–13688.

Sunshine J. M., Pieters C. M., and Pratt S. F. 1990. Deconvolution of mineral absorption bands: An improved approach. *Journal of Geophysical Research* 95:6955–6966.

Ueda Y., Miyamoto M., Mikouchi T., and Hiroi T. 2003. Surface material analysis of the S-type asteroids: Removing the space weathering effect from reflectance spectrum (abstract #2078). 34th Lunar and Planetary Science Conference. CD-ROM.

Wasson J. T. 1990. Ungrouped iron meteorites in Antarctica: Origin of anomalously high abundance. *Science* 249:900.

Xu S., Binzel B. P., Burbine T. H., and Bus S. J. 1995. Small main-belt asteroid spectroscopic survey: Initial results. *Icarus* 115:1–35.

Yamada M., Sasaki S. Nagahara H., Fujiwara A. Hasegawa S., Yano H., Hiroi T., Ohashi H., and Otake H. 1999. Simulation of space weathering of planet-forming materials: Nanosecond pulse laser irradiation and proton implantation on olivine and pyroxene samples. *Earth, Planets, and Space* 51:1255–1265.

Zolensky M. E., Weisberg M. K., and Mittlefehldt D. W. 1996. Mineralogy of carbonaceous chondrite clasts in HED achondrites and the moon. *Meteoritics & Planetary Science* 31:518.